

**Electron induced chemistry of Thioformaldehyde**

Journal:	<i>RSC Advances</i>
Manuscript ID	RA-ART-09-2015-019662.R1
Article Type:	Paper
Date Submitted by the Author:	11-Nov-2015
Complete List of Authors:	Limbachiya, Chetan; The M. S. University Baroda, Vadodara - 390001, Department of applied Physics CHAUDHARI, ASHOK; Government Engineering College Patan,, PHYSICS DESAI, HARDIK; DEPARTMENT OF PHYSICS, SARDAR PATEL UNIVERSITY, VALLABH VIDYANAGAR, PHYSICS VINODKUMAR, MINAXI; V.P & R.P.T.P. SCIENCE COLLEGE, ELECTRONICS; P.G. DEPARTMENT OF PHYSICS, SARDAR PATEL UNIVERSITY, PHYSICS
Subject area & keyword:	Biophysics - Physical < Physical

Electron induced chemistry of Thioformaldehyde

Chetan Limbachiya^a, Ashok Chaudhari^b, Hardik Desai^c and Minaxi Vinodkumar^{*d}

Received Xth XXXXXXXXXXXX 20XX, Accepted Xth XXXXXXXXXXXX 20XX

First published on the web Xth XXXXXXXXXXXX 200X

DOI: 10.1039/b000000x

A comprehensive theoretical study is carried out for electron interactions with thioformaldehyde (H_2CS) over a wide range of impact energies (0.01 eV to 5000 eV). Owing to wide energy range we have been able to compute target properties and investigate variety of processes and report data on resonances, vertical electronic excitation energies, differential cross sections (DCS), momentum transfer cross sections (MTCS), total ionization cross sections (TICS) and total cross sections (TCS) as well as scattering rate coefficients. Due to complexity involved in scattering calculations, two different theoretical formalisms are used. We have employed ab initio R-matrix method (0.01 eV to ~ 20 eV) and the spherical complex optical potential (SCOP) method (~ 20 eV to 5000 eV) to compute the cross sections. The R-matrix calculations are performed using close coupling approximation employing static exchange plus polarization (SEP) model with the aid of basis sets, 6-31G* (14 target states) and cc-pVTZ (16 target states). The target properties reported using quantum chemistry codes find good accord with earlier reported data. The scattering rate coefficients, total ionization cross sections, DCS, MTCS and TCS data (beyond 10 eV) are our maiden efforts. Further, no experimental data is available for all TCS to the best of our knowledge. We have compared all our results with available data wherever possible in literature and found overall good agreement. Due to scarcity of TCS data for thioformaldehyde, we have made comparisons with other aldehydes such as formaldehyde and acetaldehyde and drawn fruitful conclusion.

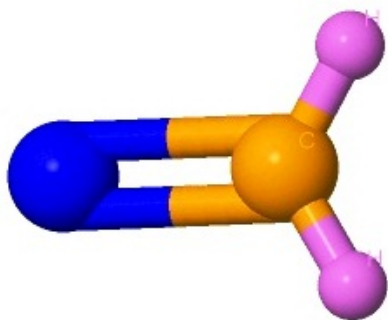


Fig. 1 (color online): Schematic diagram of H_2CS molecule

1 Introduction

Thioformaldehyde (H_2CS), is the simplest molecule (Fig. 1) in the thiocarbonyl family. It is an asymmetric rotor

^a Department of applied Physics, The M. S. University Baroda, Vadodara - 390001, India.; E-mail: chetanlimbachiya2@yahoo.com

^b Government Engineering College Patan, Gujarat - 384 265, India; E-mail: akc12878@yahoo.com

^c Department of Physics, Sardar Patel University, Vallabh Vidyanagar - 388120, India; E-mail: hardikdesai.phy@gmail.com; E-mail: p.c.vinodkumar@gmail.com

^d V P & R P T P Science College, Vallabh Vidyanagar - 388 120, India; E-mail: minaxivinod@yahoo.co.in

analogous to CH_2CN having two interchangeable hydrogen nuclei so that its rotational levels are grouped into ortho and para with statistical weights 3:1¹. Its presence in the dark clouds, interstellar clouds was noticed by many astronomical groups²⁻⁴. Recently, presence of thioformaldehyde was also detected for the first time in the circumstellar envelope around an asymptotic giant branch (AGB) star¹. Presence of thioformaldehyde in both interstellar clouds and carbon rich AGB star has motivated interest of many astrochemists to focus their study on this molecule. Further, chemical importance of H_2CS is enhanced by its significant role in the photochemical evolution of sulfur-containing species in atmospheric chemistry and astronomical systems¹⁻⁷. In fact the gas phase medium is responsible for enhancement in formation of different molecules from simple precursors by electron interaction. Thus our study for ingredients of life and understanding the origin of life on earth and other earth-like systems is geared up by electron interactions with these interstellar molecules at low and intermediate energies.

Reviewing of the literature of thioformaldehyde reveals that quantum chemical studies have concentrated their attention on molecular structures, vibrational frequencies and electronic excitation energies. The lowest vibrational transition energies 1.80 eV for transition $X\ 1A_1 \rightarrow 3A_2$ and 2.03 eV for transition $X\ 1A_1 \rightarrow 1A_2$ were first reported by Judge and King⁹ and Judge et. al.¹⁰ respectively. Furthermore, electron transitions

to the higher excited states from the ground state $1A_1$ ($\pi \rightarrow \pi^*$) and $1B_2$ ($n \rightarrow 4s$), $1A_1$ ($n \rightarrow 4p_y$), and $1B_2$ ($n \rightarrow 4p_z$) were reported at 5.60 eV, 5.84 eV, 6.60 eV, and 6.82 eV respectively by Drury and Moule¹¹. Chiang et. al.¹² and Wu et. al.¹³ carried out on the valence to Rydberg state transitions. Computationally, there are large number of multi-reference configuration-interaction (MR-CI) studies on the spectroscopy of thioformaldehyde¹⁴⁻¹⁹. More recently Wang and Tian²⁰ reported electron impact integral cross sections using R-matrix method from 0 to 10 eV. Thus literature survey makes it very clear that the study is restricted to ground state and low lying electronic excited states while the data on electron impact scattering cross sections of thioformaldehyde is very scanty. Moreover, there are no experimental data (as thioformaldehyde is unstable at room temperature and readily trimerizes to s-trithiane⁹ and hence difficult to handle experimentally) or computed data (beyond 10 eV) on Differential Cross Sections (DCS), Momentum Transfer Cross Sections (MTCS) and Total Cross Sections (TCS) to the best of our knowledge. A theoretical investigation therefore appears to be highly desirable in order to fill this void of scattering data and to understand the electron induced chemistry of this target.

The aim of the present study is many fold; (1) to detect the resonances or transient negative ion formation which are key clues at low energies for proper understanding of the anion formation, fragmentation and dissociation of the target leading to better comprehension of the target structure and electron induced local chemistry of the target, (2) to make meaningful comparison with earlier reported data and (3) to fill the void of the collision data as earlier data is sparse. Further, due to scarcity of total cross section data for thioformaldehyde we have compared our TCS data with other aldehydes viz. formaldehyde²¹ and acetaldehyde²².

2 METHODOLOGY

A single theoretical formalism cannot be employed to encompass the diverse physical phenomena occurring at low and intermediate to high energy scattering. Hence, for the low impact energies (0.01 eV to about 20 eV) we performed an ab initio calculation using UK molecular R-matrix code²⁴ and used Spherical Complex Optical Potential formalism for intermediate to high energies. At low impact energies the total cross section is a sum of total elastic and total electronic excitation (inelastic contribution) cross sections, while at intermediate to high energies the total cross section is a sum of total elastic and total excitation plus ionisation (inelastic contribution) cross sections. These two formalisms are briefly outlined in the following subsections. The accuracy of low energy calculations is largely dependent on the target model

employed. Hence, before discussing the theoretical methods we first furnish the details of target model employed for the present system.

2.1 TARGET MODEL

Correct description of the electronic states of the target molecule obtained from the target wavefunction is fundamental step to obtain meaningful and accurate collision data. Thioformaldehyde, H_2CS is an α -type asymmetric top molecule with C_{2v} point group symmetry. We have used following geometry in the present calculations²⁵; bond lengths, $R(C=S)=1.611 \text{ \AA}$, $R(C-H)=1.087 \text{ \AA}$, and bond angles $(H-C-H)=116.52^\circ$, $(H-C-S)=121.74^\circ$. The Hartree-Fock electronic configuration for the ground state of H_2CS at its equilibrium geometry in C_{2v} symmetry is $1a'^2, 2a'^2, 3a'^2, 4a'^2, 1b''^2, 1b'^2, 5a'^2, 6a'^2, 2b''^2, 2b'^2, 3b''^2, 3b'^2$ using 6-31G* as well as cc-pVTZ basis sets. In order to preserve balance between the amount of correlation incorporated in the target wavefunction and in the scattering calculation, out of 24 electrons, 16 electrons are frozen in eight molecular orbitals ($1a', 2a', 3a', 4a', 5a', 6a', 1b', 1b''$) and 8 electrons are kept free to move in active space of seven molecular orbitals ($7a', 8a', 2b', 3b', 2b'', 3b'', 4b''$). We have used cc-pVTZ and 6-31G* basis sets in order to study the dependency of target properties and scattering cross sections on the basis set chosen. The lowest remaining virtual orbitals for each symmetry were used to augment the continuum basis by allowing scattering electron to occupy them.

The major parameters involved in careful choice of the configurations are complete active space (CAS) and the valance configuration interaction (CI) representation of the target system²⁶. The CAS-CI model uses the complete active space with self-consistent field (SCF) orbitals optimized on the ground state. The molecular orbitals are generated by performing a SCF calculation of the ground state of the molecule ($X1A_1$). Since the SCF procedure is inadequate to provide a good representation of the target states, we improve the energies of these states by invoking the variational method of configuration interaction (CI) in which we take linear combination of configuration state functions (CSFs) of a particular overall symmetry. This lowers the energies and the correlation introduced provides a better description of the charge cloud and the energies. For all the states included here, we employ CI wave function to represent the target states.

The Born correction for this polar molecule is employed to account for higher partial waves, $l > 4$. In the static-exchange-polarization (SEP) model, the ground state of the molecule is perturbed by single and double excitations of the electrons, thus leading to the inclusion of polarization effects.

Thus polarization effects are accounted by including closed channels in a CI expansion of the wave function of the entire scattering system.

The GAUSPROP and DENPROP modules²⁷ construct the transition density matrix from the target eigenvectors obtained from Configuration Integration (CI) expansion and generate the target properties. The multipole transition moments obtained are then used to solve the outer region coupled equations and the dipole polarizability α_0 . These are computed using second-order perturbation theory and the property integrals are evaluated by GUASPROP²⁷. Our self-consistent field (SCF) model calculations yielded target properties such as the ground state energy, the first electronic excitation energy, rotational constant and dipole moment. These are listed in Table 1.

Self-consistent field calculations yielded the ground state energy of -436.517 Hartree using 6-31G* and -436.553 Hartree using cc-pVTZ basis sets. The ground state energies obtained using 6-31G* is close to -436.513 Hartree reported by Wang and Tian²⁰ and -436.506 reported by Goddard²⁸. The ground state energy obtained using 6-31G* is -436.517 Hartree which is close to both the predicted values^{20,28}. We report 14 and 16 electronic excitation states below ionization threshold of the target using 6-31G* and cc-pVTZ basis sets respectively for thioformaldehyde with the first electronic excitation energy obtained at 1.88 eV using 6-31G* and 1.76 eV using cc-pVTZ basis sets. First electronic excitation energy of 1.88 eV using 6-31G* and 1.76 eV using cc-pVTZ is in good accord with the experimental value of 1.80 eV reported by Judge et. al.¹⁰ and theoretical value of 1.84 eV reported by Bruna et. al.¹⁴. The present rotational constant, 9.8597 cm^{-1} is slightly higher than 9.6399 cm^{-1} of Wang and Tian²⁰ and in good agreement with experimental value 9.7272 cm^{-1} reported by Clouthier et. al.²⁹ and 9.7304 cm^{-1} by Johnson et. al.³¹. The rotational constant values (B and C) are close to the corresponding experimental values reported by Johnson et. al.³¹ as clear from Table 1. The dipole moment obtained through our calculations are 1.7780 D using 6-31G* and 2.2022 D using cc-pVTZ basis sets. Our dipole moment value using 6-31G* is 1.7780 D and is in good accord with theoretical value of 1.7979 D²⁰, experimental values of 1.6491 D³⁰ and 1.6474 D³¹. It can be easily seen that dipole moment is sensitive to the basis set and the target model chosen. The 6-31G* and cc-pVTZ basis sets give very good accord for all the target properties except for dipole moment using cc-pVTZ basis set.

The electronic and angular momentum channels altogether generated 615 configuration state functions (CSFs) and 84 channels in the calculation. In Table 2 we have reported

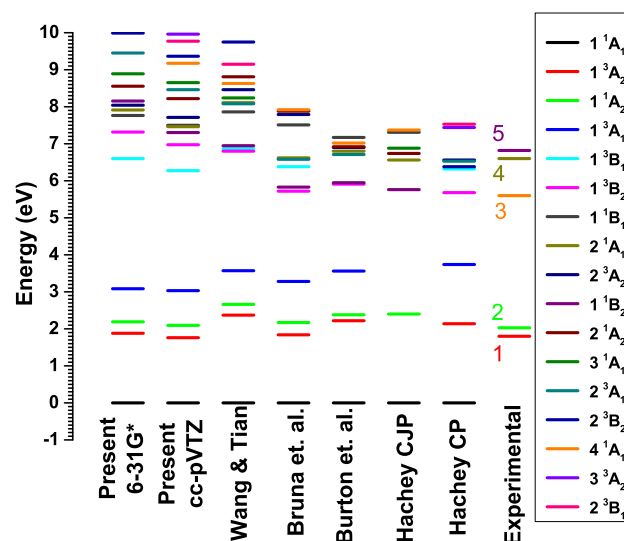


Fig. 2 (color online): Schematic diagram for vertical excitation energies for Present calculations using 6-31G* and cc-pVTZ basis sets in comparison of earlier reported theoretical data by Wang & Tian²⁰, Bruna et. al.¹⁴, Burton & Peyerimhoff¹⁵, Hachey et. al. (CJP¹⁶ & CP¹⁷) and experimental data: 1 - Judge et. al.¹⁰; 2 - Judge & King⁹; 3,4 and 5 - Drury & Moule¹¹

14 lowest electronic excited states (1^1A_1 , 3^3A_2 , 1^1A_2 , 3^3A_1 , 3^3B_1 , 3^3B_2 , 1^1B_1 , 1^1A_1 , 3^3A_2 , 1^1B_2 , 1^1A_2 , 1^1A_1 , 3^3A_1 and 3^3B_2) using 6-31G* basis set and 16 electronic excited states (1^1A_1 , 3^3A_2 , 1^1A_2 , 3^3A_1 , 3^3B_1 , 3^3B_2 , 1^1B_1 , 1^1A_1 , 3^3A_2 , 1^1B_2 , 1^1A_2 , 1^1A_1 , 3^3A_1 , 3^3B_2 , 3^3B_1 and 3^3A_2) using cc-pVTZ basis sets. The 14 (6-31G*) and 16 (cc-pVTZ) electronic excited target states employed all possible single and double excitations to virtual orbitals. There are many previous studies on electronic excitations of thioformaldehyde^{9-12,14-17} compared vide Table 2 and also presented graphically vide figure 2.

2.2 Low energy formalism (0.01 ~ 15 eV)

Three most popular methodologies viz. Kohn variational method^{34,35}, Schwinger multichannel method^{36,37}, and R-matrix method²⁴ are in use for performing low energy electron collision calculations. Out of these three popular methods, R matrix is the most widely used method. The basic idea underlying the R-matrix method²⁴ is partition of the configuration space into an inner region, which corresponds to a sphere of radius 'a' whose centre is centre of mass of the target molecule and an outer region. Radius of the R-matrix sphere is chosen to be large enough that the charge density of the target is completely embedded in the inner region and

Table 1 Target properties obtained for the Thioformaldehyde molecule using 6-31G* and cc-pVTZ basis sets

Target Property	Present		Other	
	6-31G*	cc-pVTZ	Theory	Experiment
Ground State Energy (Hartree)	-436.517	-436.553	-436.513 ²⁰ -436.506 ²⁸	
First excitation energy (eV)	1.88	1.76	1.84 ¹⁴ , 2.14 ¹⁷ 2.22 ¹⁵ , 2.37 ²⁰	1.80 ¹⁰
Rotational Constant (cm^{-1})				
	A	9.8597	9.8597	9.7272 ²⁹ 9.7304 ³¹
	B	0.5932	0.5932	0.5915 ²⁰ 0.5904 ³¹
	C	0.5595	0.5595	0.5573 ²⁰ 0.5555 ³¹
Dipole moment (Debye)		1.7780	2.2022	1.7979 ²⁰ 1.6491 ³⁰ 1.6474 ³¹

Table 2 Vertical excitation energies (eV) for H_2CS below 10 eV for 6-31G* and cc-pVTZ basis sets

State	Present		Other Cal.				Exp.	
	6-31G*	cc-pVTZ	Wang & Tian ²⁰	Bruna et. al. ¹⁴	Burton & Peyerimhoff ¹⁵	Hachey & Grein ¹⁶		Hachey & Grein ¹⁷
1 ¹ A ₁	0.00	0.00	0.00	0.00	0.00	0.00	0.00	-
1 ³ A ₂	1.88	1.76	2.37	1.84	2.22	-	2.14	1.80 ¹⁰
1 ¹ A ₂	2.19	2.09	2.66	2.17	2.38	2.4	-	2.03 ⁹
1 ³ A ₁	3.08	3.03	3.57	3.28	3.56	-	3.74	-
1 ³ B ₁	6.60	6.27	6.87	6.38	-	-	6.32	-
1 ³ B ₂	7.32	6.98	6.80	5.72	5.91	-	5.68	-
1 ¹ B ₁	7.76	7.50	7.86	7.51	7.17	7.31	-	-
2 ¹ A ₁	7.91	7.46	8.11	6.62	6.80	6.56	-	6.60 ¹¹ , 5.72 ³²
2 ³ A ₂	8.04	7.71	8.46	7.79	6.90	-	6.56	-
1 ¹ B ₂	8.15	7.30	6.95	5.83	5.95	5.76	-	5.84 & 6.82 ¹¹ , 5.83 ³² 5.845 ¹² , 5.86 ³³
2 ¹ A ₂	8.55	8.22	8.81	7.88	6.92	6.74	-	-
3 ¹ A ₁	8.89	8.65	8.24	-	-	6.88	-	-
2 ³ A ₁	9.45	8.46	8.08	6.58	6.71	-	6.53	-
2 ³ B ₂	9.99	9.37	9.75	-	-	-	6.38	-
4 ¹ A ₁	-	9.18	8.63	7.92	7.02	7.37	-	5.60 ¹¹
3 ³ A ₂	-	9.96	-	-	-	-	7.44	-
2 ³ B ₁	-	9.77	9.15	-	-	-	7.53	-

exchange and electron-electron correlation are important and are to be handled with utmost care. In the external region, short range forces (electron electron correlation and exchange) become negligible and only known long-range forces are effective. The continuum orbitals are orthogonalized to the target orbitals by diagonalizing the overlap matrix and discarding vectors with eigenvalues less than 1×10^{-7} . The continuum basis in our calculations is not constrained to R-matrix sphere and hence no Buttle corrections are required. In the inner region full electron-molecule problem is solved using Quantum Chemistry codes which takes almost 90% of the total computational time. The advantage of R-matrix method originates from the fact that the electronic Hamiltonian needs only be diagonalised once to obtain scattering wave function for any energy up to a certain maximum of scattering energy. The inner region is usually chosen to have a radius of 10 au and the outer region is extended to about 100 au. The choice of this value depends on the stability of results obtained in the inner region and outer region calculations and proper reproduction of target properties. We describe the scattering within the fixed-nuclei (FN) approximation that neglects any dynamics involving the nuclear motion (i.e. rotational as well as vibrational), whereas the bound electrons are taken to be in the ground electronic state of the target at its optimized nuclear geometry. This is an effect of the extent of electronic charge density distribution around the center of mass of the target. In the present study we have considered inner R-matrix radius as 10 au for all target models.

In the inner region the total wave function for the system is written as,

$$\Psi_k^{N+1} = A \sum_I \Psi_I^N(x_1, \dots, x_N) \sum_j \zeta_j(x_{N+1}) a_{Ijk} + \sum_m \chi_m(x_1, \dots, x_{N+1}) b_{mk} \quad (1)$$

Where, A is an antisymmetrization operator introduced so that the indistinguishable inner-region electrons satisfy the Pauli's exclusion principle, x_N are the spatial and spin coordinates of the n^{th} target electron, ζ_j is a continuum orbital spin-coupled with the scattering electron with a partial wave expansion up to some maximum value of l , say l_{max} , a_{Ijk} and b_{mk} are variationally optimized coefficients. The summations in the first term runs over the number of target states used in the close-coupled expansion. The second summation in equation 1 runs over configurations χ_m , which describe all N+1 electrons but vanish at $r = a$; thus these are described as L^2 configurations. The occupancy of the virtual orbitals of the target, corresponding to the second term of equation 1, is necessary to complete the wavefunction space of the scattering electron, which is restricted by the orthogonalization of the continuum orbitals to the target orbitals. The target wavefunctions are usually determined from CI calculation, where a wave func-

tion is expanded as linear combination of configuration state functions (CSFs) given by

$$\Psi_k^N = \sum_i C_{ki} \phi_i^N \quad (2)$$

The expansion coefficient C_{ki} are such that they diagonalise the target Hamiltonian matrix in the basis of the generated CSFs, ϕ_i^N . The target molecular orbitals used to construct the CSFs are optimised using the Hartree Fock self consistent field method using Gaussian type orbitals.

In the inner region calculations, polarization effects are considered employing the second sum in equation 1 using singly excited L^2 configurations of the Hartree-Fock (HF) ground state wave function. This is achieved by promoting one target electron into a virtual (unoccupied target) orbital and simultaneously also placing the scattering electron into a virtual orbital generating a two-particle one-hole (2p,1h) configuration. This model is usually denoted as static exchange plus polarization (SEP). This is underlying assumption which allows one to ignore exchange in the outer region but excludes the possibility to treat electron impact ionization. The excitation cross sections from the molecular ground state to a few low-lying excited states have also been calculated, and these excited states formed in the inelastic collisions can decay into the ground state with photon emissions or by coupling with the dissociation channels to produce the anionic and neutral fragments.

The target and the continuum orbitals are represented by Gaussian Type Orbitals (GTOs) and the molecular integrals are generated by the appropriate Molecular Package. The R-matrix will provide the link between the inner region and outer region. For this purpose the inner region is propagated to the outer region until its solutions match with the asymptotic functions which are largely obtained from the Gaillitis expansion²⁴. Thus by generating the wave functions, using Eq. 2, their eigenvalues are determined. These coupled single centre equations describing the scattering in the outer region are integrated to identify the K - matrix elements. The K - matrix is a symmetric matrix whose dimensions are the number of channels. All the observable are basically deduced from it and further it is used to deduce T matrix using the relation:

$$T = \frac{2iK}{1 - iK} \quad (3)$$

The T - matrices are in turn used to obtain various total cross sections. The K - matrix is diagonalized to obtain the eigenphase sum. The eigenphase sum is further used to obtain the position and width of the resonance by fitting them to the Breit Wigner profile³⁸ using the program RESON³⁸.

POLYDCS program³⁹ is employed to compute differential cross sections (DCS) and momentum transfer cross sections (MTCS). Differential Cross section study is very important as it provides important information about the various interaction processes occurring between the target and incoming electron. Indeed, the evaluation of DCS is stringent test for any scattering theory as it is sensitive to effects which are averaged out in integral cross sections. The DCS for polyatomic molecule is represented by:

$$\frac{d\sigma}{d\Omega} = \sum_L A_L P_L(\cos\theta) \quad (4)$$

where, P_L represents the Legendre polynomial of order L. The details about A_L are discussed by Gianturco and Jain⁴⁰. For a polar molecule this expansion over L converges slowly owing to the long range nature of dipole potential. To overcome this problem we use the closure formula given by:

$$\frac{d\sigma}{d\Omega} = \frac{d\sigma^B}{d\Omega} + \sum_L (A_L - A_L^B) P_L \cos\theta \quad (5)$$

Here the subscript, B denotes the fact that the relevant term is calculated under Born Approximation with an electron point dipole interaction. It is clear from the expression 5 that convergence of the series is faster as the contribution arising from Born term is subtracted as seen in Eqn. 5. The quantity $\frac{d\sigma^B}{d\Omega}$ for any initial rotor state is given by the sum over all final rotor states as

$$\frac{d\sigma^B}{d\Omega} = \sum_{J'\tau'} \frac{d\sigma^B}{d\Omega} (J\tau \rightarrow J'\tau') \quad (6)$$

The calculated dipole moment (1.88 D) and rotational constants ($A=9.8597 \text{ cm}^{-1}$, $B=0.5932 \text{ cm}^{-1}$, $C=0.5595 \text{ cm}^{-1}$) for H_2CS are used in the calculation of elastic DCS ($J=0 \rightarrow J'=0$) and rotationally inelastic ($J=0 \rightarrow J' = 1, 2, 3, 4$ and 5) DCSs at different collision energies.

In fact the MTCS is obtained by integrating the differential cross sections (DCS) with a weight factor $(1-\cos\theta)$.

$$\sigma_m = 2\pi \int \frac{d\sigma}{d\Omega} (1-\cos\theta) d\theta \quad (7)$$

2.3 Higher energy formalism (Threshold to 5 keV)

Close coupling formalism cannot be employed beyond 20 eV as many channels are open beyond this energy and the size of matrices become so large that their solution are beyond the scope of present day computational facilities. Hence above the ionization threshold energy of the target, scattering calculations are performed using the SCOP formalism^{41,44}. In this formalism, the electron-molecule system is represented

by a complex optical potential which could be effectively represented in terms of real and imaginary parts as,

$$V_{opt}(r, E_i) = V_R(r) + iV_I(r, E_i) \quad (8)$$

such that,

$$V_R(r, E_i) = V_{st}(r) + V_{ex}(r, E_i) + V_p(r, E_i) \quad (9)$$

where, E_i is the incident energy of the incoming electron. Eq. 9 corresponds to various real potentials to account for the electron target interaction namely, static, exchange and polarization potentials respectively. These potentials are functions of the target geometry, the molecular charge density of the target, the ionization potential and the polarizability of the target. The molecular charge density may be derived from the atomic charge density by expanding it at the center of mass of the system. The molecular charge density so obtained is renormalized to account for the total number of electrons present in the target. The atomic charge densities and static potentials (V_{st}) are formulated from the parameterized Hartree-Fock wave functions given by Cox and Bonham⁴⁵.

The parameter free Hara's 'free electron gas exchange model'⁴⁶ is used for the inclusion of exchange potential (V_{ex}). The exchange potential takes care of exchange of scattering electron with one of the target electrons. The polarization potential (V_p) is formulated from the parameter free model of correlation-polarization potential given by Zhang et. al.⁴⁷. Here, various multipole non-adiabatic corrections are incorporated in the intermediate region which will approach the correct asymptotic form at large 'r' smoothly. The target parameters like ionization potential (I) and dipole polarizability (α_0) of the target used here are the best available from the literature⁴⁸.

The imaginary part in V_{opt} , called the absorption potential V_{abs} accounts for the total loss of flux from the incident channel, scattered into the allowed electronic excitation or ionization channels. The expression used here are vibrationally and rotationally elastic. This is due to the fact that the non-spherical terms do not contribute much to the total potential at the present high energy range.

The well-known quasi-free model of Staszeweska et. al.⁴⁹ is employed for the absorption part, given by,

$$V_{abs}(r, E_i) = -\rho(r) \sqrt{\frac{T_{loc}}{2}} \left(\frac{8\pi}{10k_F^3 E_i} \right) \times \theta(p^2 - k_F^2 - 2\Delta)(A_1 + A_2 + A_3) \quad (10)$$

Where T_{loc} is the local kinetic energy of the incident electron which is given by,

$$T_{loc} = E_i - (V_{st} + V_{ex} + V_p) \quad (11)$$

Here $p^2 = 2E_i$ and $k_F = [3\pi^2\rho(r)]^{\frac{1}{3}}$ is the Fermi wave vector and A_1 , A_2 and A_3 are dynamic functions that depend differently on $\theta(x)$, I , Δ and E_i . These three parameters A_1 , A_2 and A_3 are explicitly given in our earlier publication⁴³ and hence not repeated here. Here, I is the ionization threshold of the target, $\theta(x)$ is the Heaviside unit step-function and Δ is an energy parameter below which $V_{abs} = 0$. Hence, Δ is the principal factor which decides the values of total inelastic cross section, since below this value ionization or excitations are not allowed. This is one of the main characteristics of Staszewska model⁴⁹. This has been modified by us by considering Δ as a slowly varying function of E_i around I . Such an approximation is meaningful since Δ fixed at I would not allow excitation at energies $E_i \leq I$. However, if Δ is much less than the ionization threshold, then V_{abs} becomes unexpectedly high near the peak position. The amendment introduced is to give a reasonable minimum value $0.8I$ to Δ ⁵⁰ and also to express the parameter as a function of E_i around I , i.e.,

$$\Delta(E_i) = 0.8I + \beta(E_i - I) \quad (12)$$

Here the parameter β is obtained by requiring that $\Delta = I$ (eV) at $E_i = E_p$, the value of incident energy at which present Q_{inel} reaches its peak. E_p can be found by calculating Q_{inel} by keeping $\Delta = I$. Beyond E_p , Δ is kept constant and is equal to I . The expression given in Eqn. 12 is meaningful as Δ fixed at the ionization potential would not allow any inelastic channel to open below I . Also, if it is much less than I , then V_{abs} becomes significantly high close to the peak position of Q_{inel} .

The complex potential thus formulated is used to solve the Schrödinger equation numerically through partial wave analysis. This calculation will produce unique complex phase shift for each partial wave which carries the signature of interaction of the incoming projectile with the target. At low energies only a few partial waves (5-6 for absorption and 100 for polarization at ionization threshold) are significant, but as the incident energy increases more partial waves (around 40 for absorption and 100 for polarization) are needed for convergence. The phase shifts δ_l thus obtained are employed to find the relevant cross sections, total elastic (Q_{el}) and the total inelastic cross sections (Q_{inel}) using the scattering matrix $S_l(k) = \exp(2i\delta_l)$ ⁵¹. Then the total scattering cross section (TCS), Q_T is obtained by adding these two cross sections⁵¹.

The important ionization channel is embedded in the total inelastic channel. We have computed total ionization cross sections using complex scattering potential-ionization contribution (CSP-ic) method⁵²⁻⁵⁴ and Binary Encounter Bethe (BEB) methods⁵⁵, since there are no theoretical or experimental data reported to the best of our knowledge. Both the methods (CSP-ic and BEB) are well established and we have reported ionization cross sections of varied targets

successfully using CSP-ic method^{52,53}.

3 RESULTS AND DISCUSSION

The present work reports detailed study on electron induced chemistry on H_2CS over a wide range of impact energies. Such a wide range includes diverse phenomena and accordingly we have reported data on resonances, electronic excitations, differential, momentum transfer, ionization and total cross sections along with scattering rate coefficients. We have employed the ab initio R matrix code below 20 eV. The total cross section is sum of total elastic and total electronic excitation (inelastic part) cross sections below the ionization threshold of the target. Above the threshold, we have computed the total cross section as the sum of total elastic and total inelastic cross section using the SCOP formalism^{41,44}. With amalgamation of these two methodologies, we are able to predict the total cross sections over wide energy range from 0.01 eV to 5000 eV^{42,43,56}.

One of the important tasks at low impact energies is the generation of eigenphase sum as it provides the position and width of resonances which are important features of collision study. Transient negative ion formation or resonances are a common characteristic of electron molecule scattering at low impact energies and leads to distinctive structure in pure vibrational excitation cross sections⁵⁷ leading to knowledge of decay channels of the target. A recursive procedure for detecting and performing Breit Wigner fits³⁸ to the eigenphase diagram is done through program RESON³⁸. The detailed procedure is described in our earlier publications^{42,43,56} and hence not repeated here.

Temporary negative ions in general cause structure in the inelastic cross-sections, and the energy dependence of the various inelastic processes thus represents a convenient way to obtain a global view of the negative ion states. Table 3 shows the resonances detected in A', A'', B' and B'' symmetries. This study is carried out earlier only by Wang and Tian²⁰. Doublet B'' state shows a broad core excited shape resonance structure at 2.9368 eV and 2.7008 eV with corresponding width of 0.2983 eV and 0.2700 eV using 6-31G* and cc-pVTZ basis sets respectively. This resonance is close to resonance at 3.62 eV observed by Wang and Tian²⁰. Second core excited resonance predicted by 2B' symmetry state is at 4.6968 eV with a width of 0.7839 eV obtained using 6-31G* basis set and at 4.5170 eV with a width of 0.6826 eV using cc-pVTZ basis set are close to earlier reported core excited resonance at 5.15 eV with a width of 1.1696 eV by Wang and Tian²⁰. Feshbach resonance observed due to doublet A' symmetry at 7.6588 eV and at 7.1252 eV using 6-31G* and cc-pVTZ

Table 3 Position and width (both in eV) of resonance states calculated using 6-31G* and cc-pVTZ basis sets

State	Present Position		Other Position ²⁰	Present Width		Other Width ²⁰
	6-31G*	cc-pVTZ		6-31G*	cc-pVTZ	
A'	7.6588	7.1252	6.94	0.0001	0.2158	0.0304
		8.4409	7.98		0.0097	0.037
		14.6723			0.1498	
	17.3926	17.2945		0.8820	0.4294	
B'	18.9249	19.2953		0.1172	0.1332	
	4.6968	4.5170	5.15	0.7839	0.6826	1.1696
	18.6754	18.0335		0.4961	0.2093	
B''		19.0331			0.1952	
	2.9368	2.7008	3.62	0.2983	0.2700	0.5698
	15.8258	15.0914		5.8×10^{-6}	0.2541	
A''	17.0020	15.2362		0.3691	0.1050	
	17.2489	16.1342		0.1914	0.2424	
		15.0420			0.0546	
	18.2218			0.1543		

basis sets respectively are close to resonance observed at 6.94 eV and 7.98 eV reported by Wang and Tian²⁰. The resonances predicted above 10 eV are not found in the literature to the best of our knowledge and hence predicted for the first time as evident from the table 3. Thus the eigenphase study provides us detailed knowledge about the resonances of thioformaldehyde. Table 3 gives the positions and widths of resonances obtained in the present case using R-matrix calculations.

Figure 3 presents electron-impact excitation cross sections from the ground state (X^1A_1) to the first eight excited states (3A_2 , 1A_2 , 3A_1 , 3B_1 , 3B_2 , 1B_1 , 1A_1 and 3A_2) for impact energies 0 to 20 eV. Moreover 13 (3A_2 , 1A_2 , 3A_1 , 3B_1 , 3B_2 , 1B_1 , 1A_1 , 3A_2 , 1B_2 , 1A_2 , 1A_1 , 3A_1 and 3B_2) and 15 (3A_2 , 1A_2 , 3A_1 , 3B_1 , 3B_2 , 1B_1 , 1A_1 , 3A_2 , 1B_2 , 1A_2 , 1A_1 , 3A_1 , 3B_2 , 1A_1 , 3A_2 and 3B_2) electronic excited states are reported using 6-31G* and cc-pVTZ basis set respectively vide Table 2. First and second electronic excitation energies are in good agreement with measured values reported by Judge et. al.¹⁰ and Judge and King⁹ respectively and also with theoretical data of Bruna et. al.¹⁴ and are slightly lower than the theoretical predictions by Hachey and Grein¹⁷, Wang and Tian²⁰ Burton and Peyerimhoff¹⁵. Third electronic excitation energies are lower than the theoretical predictions of Wang and Tian²⁰, Bruna et. al.¹⁴, Burton and Peyerimhoff¹⁵ and Hachey and Grein¹⁷. This transition gives maximum excitation cross section of 1.43 \AA^2 at 4.76 eV. The excitation energies for fourth transition are close to predictions of Wang and Tian²⁰, Bruna et. al.¹⁴ and Hachey and Grein¹⁷.

Fifth transition energies are comparable with values reported by Wang and Tian²⁰ and are much higher than the predictions of Bruna et. al.¹⁴, Burton and Peyerimhoff¹⁵ and

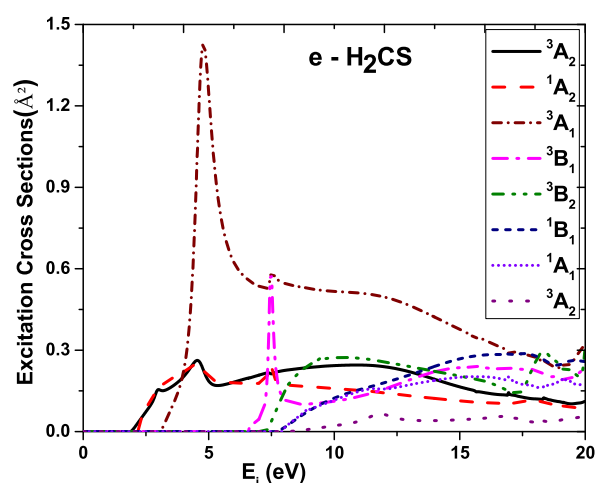


Fig. 3 (color online): Excitation cross sections from the ground state (X^1A_1) to the first eight excited states for $e-H_2CS$ scattering; Solid - 3A_2 , Dash - 1A_2 , Short dash dot - 3A_1 , Dash dot - 3B_1 , Dash dot dot - 3B_2 , Short dash - 1B_1 , Short dot - 1A_1 , Dot - 3A_2

Hachey and Grein¹⁷. Sixth and seventh transition energies are comparable with reported values by Wang and Tian²⁰, Bruna et. al.¹⁴, Burton and Peyerimhoff¹⁵ and Hachey and Grein¹⁶. Further seventh transition energies are lower than the measured value reported by Drury et. al.¹¹ and Judge et. al.³². The Eighth transition values are in very good agreement with theoretical predictions of Wang and Tian²⁰, Bruna et. al.¹⁴ and higher than the reported values by Burton and Peyerimhoff¹⁵ and Hachey and Grein¹⁶. Ninth transition values are higher than the theoretical predictions by Wang and Tian²⁰, Bruna et. al.¹⁴, Burton and Peyerimhoff¹⁵, Hachey and Grein¹⁶ and measured value of Drury et. al.¹¹, Judge³², Chiang and Lin¹² and Caller et. al.³³. Tenth transition values are close to reported values of Wang and Tian²⁰, Bruna et. al.¹⁴, and lower than the reported values of Burton and Peyerimhoff¹⁵, Hachey and Grein¹⁶. Eleventh and twelfth transition values are close to reported values of Wang and Tian²⁰ and eleventh transition energies are higher than the values of Hachey and Grein¹⁷ and twelfth transition energies are higher than Bruna et. al.¹⁴, Burton and Peyerimhoff¹⁵ and Hachey and Grein¹⁷. Thirteenth and fourteenth transitions are in good agreement with the values reported by Wang and Tian²⁰. Thirteenth transition value is higher than that reported by Hachey and Grein¹⁷ and fourteenth transition values are higher than Bruna et. al.¹⁴, Burton and Peyerimhoff¹⁵, Hachey and Grein¹⁶ and Drury et. al.¹¹. While fifteenth and sixteenth transition values are higher than the values reported by Hachey and Grein¹⁷, sixteenth transition values are in good agreement with theoretical predictions of Wang and Tian²⁰. No measurement data are reported for third, fourth, fifth, sixth, eighth, tenth, eleventh, twelfth, thirteenth, fifteenth and sixteenth transitions. All transitions are reported in Table 2. The discrepancies between our results and values reported in literature may be attributed to selection of basis sets and the target model employed for the calculation.

We have plotted DCS curves for 1 eV to 7 eV and 10 eV, 15 eV and 20 eV using 6-31G* basis set. We have clubbed the DCS for 1eV and 7 eV in figure 4 for comparison with available data of Wang and Tian²⁰. Figure 4 shows comparison of our DCS at 1 eV for the sum total of all transitions ($J = 0$ to $J' = 0$ to 5) compared with theoretical results of Wang and Tian²⁰. There is no other theoretical or experimental comparison to the best of our knowledge. The total DCS at 1 eV is dominated by the dipole component ($J = 0 \rightarrow J' = 1$). As H_2CS is a polar molecule, the dipole component ($J = 0 \rightarrow J' = 1$) is much larger than the elastic component ($J = 0 \rightarrow J' = 0$). The calculated DCS is converged when J' increases up to 5. Moreover, in the elastic component, there is a strong minimum at about 132° . The results of Wang and Tian²⁰ are qualitatively and quantitatively in good agreement with present results for all angles. Our DCS data for 7 eV finds

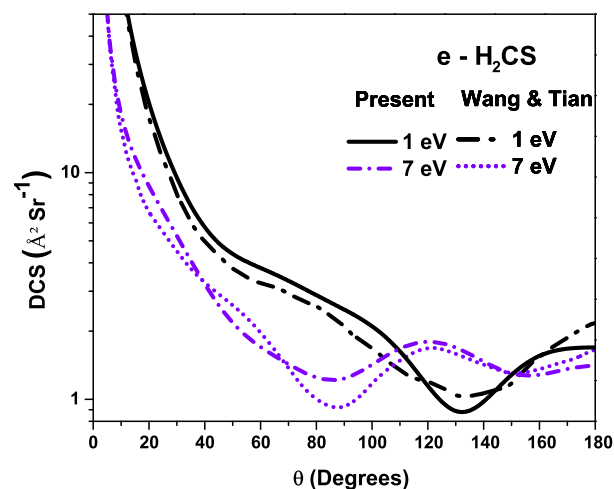


Fig. 4 (color online): Differential Cross Sections (DCS) for incident energies of 1 eV and 7 eV; Present: Solid - 1 eV, Short dash dot - 7 eV; Wang & Tian²⁰: Dash dot - 1 eV, Short dot - 7 eV

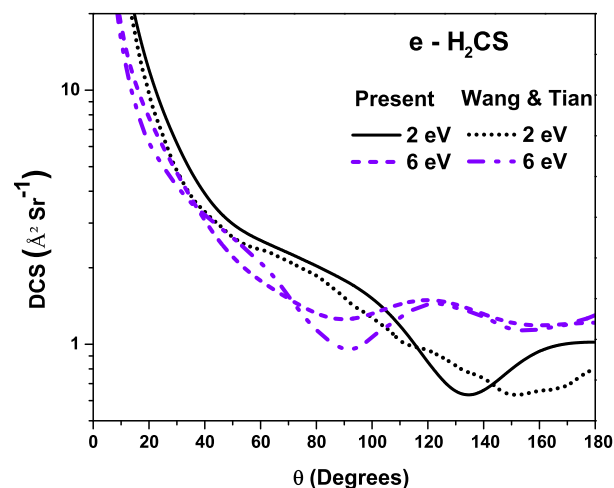


Fig. 5 (color online): Differential Cross Sections (DCS) for incident energies of 2 eV and 6 eV; Present: Solid - 2 eV, Short dash - 6 eV; Wang & Tian²⁰: Short dot - 2 eV, Dash dot dot - 6 eV

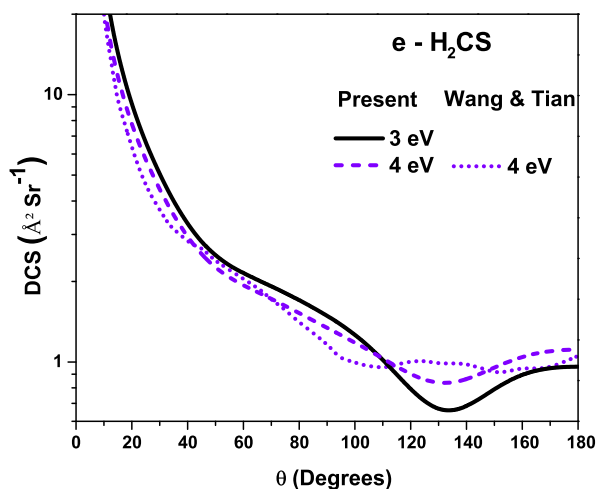


Fig. 6 (color online): Differential Cross Sections (DCS) for incident energies of 3 eV and 4 eV; Present: Solid - 3 eV, Short dash - 4 eV; Wang & Tian²⁰: Short dot - 4 eV

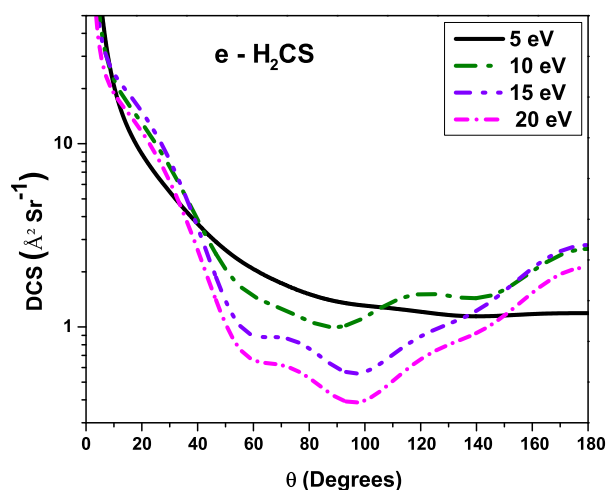


Fig. 7 (color online): Differential Cross Sections (DCS) for incident energies of 5 eV, 10 eV, 15 eV and 20 eV; Present: Solid - 5 eV, Dash dot - 10 eV, Dash dot dot - 15 eV, Short dash dot - 20 eV

very good agreement with the results of Wang and Tian²⁰ as evident from the curve and has two minima at 86° and 156°. The positions of two minima are also in good agreement with the results of Wang and Tian²⁰.

Figure 5 shows our differential cross sections summed over all transitions ($J=0$ to $J'=0$ to 5) for incident energy of 2 eV and 6 eV compared with theoretical results of Wang and Tian²⁰. The scattering is dominated by elastic component $0 \rightarrow 0$ and dipole component $0 \rightarrow 1$. For 2 eV, the elastic component shows a minimum at around 133° which indicates the dominance of a p-wave in the interference pattern arising due to various partial wave amplitudes. As the energy increases the convergence with respect to J is rapid. The divergence at the forward angle is confirmed as being due to dipole allowed transitions $0 \rightarrow 1$ dominating the scattering. The differential cross sections decrease as the incident energy increases. The sharp enhancement in the forward direction is a result of the strong long-range dipole component of the interaction potential. Our data finds qualitatively good agreement with theoretical data of Wang and Tian²⁰ for angles up to 120° and beyond this angle our data differs from that of Wang and Tian²⁰. Our 6 eV results for DCS find overall good agreement both qualitatively as well as quantitatively with the minima positions around 90° and 160°. Similarly figure 6 shows DCS curves for 3 eV and 4 eV. 3 eV curve has clear minimum at 133° and no comparison is available either theoretical or experimental. For 4 eV our DCS curve is comparable with that of Wang and Tian²⁰ till 100° beyond which they differ.

Figure 7 shows sum of our differential cross sections summed over all transitions ($J=0$ to $J'=0$ to 5) for incident energy of 5 eV, 10 eV, 15 eV and 20 eV. There are no comparisons available for DCS at these incident energies.

A further test of the quality of our DCS is shown by the momentum transfer cross section (MTCS) in figure 8 for energies 0 eV to 20 eV. In figure 8 we have reported and compared our MTCS calculated using 6-31G* and cc-pVTZ basis sets with results of Wang and Tian²⁰. The MTCS indicates the importance of the backward scattering and is an important quantity that forms the input to solve the Boltzmann equation for the calculation of electron distribution function of swarm of electrons drifting through a molecular gas. At the lower incident energies, the backward scattering is predominant, reflected through large MTCS. The divergent behavior observed in DCS in the forward direction (i.e. large scattering angle) is reduced in MTCS due to the multiplicative factor $(1 - \cos\theta)$, where θ is the scattering angle. Our MTCS data are in good agreement with theoretical data of Wang and Tian²⁰ for all impact energies reported by them. Moreover all resonances predicted through eigenphase sum are well reproduced as peaks in the MTCS curve using 6-31G* and cc-pVTZ basis sets. Ad-

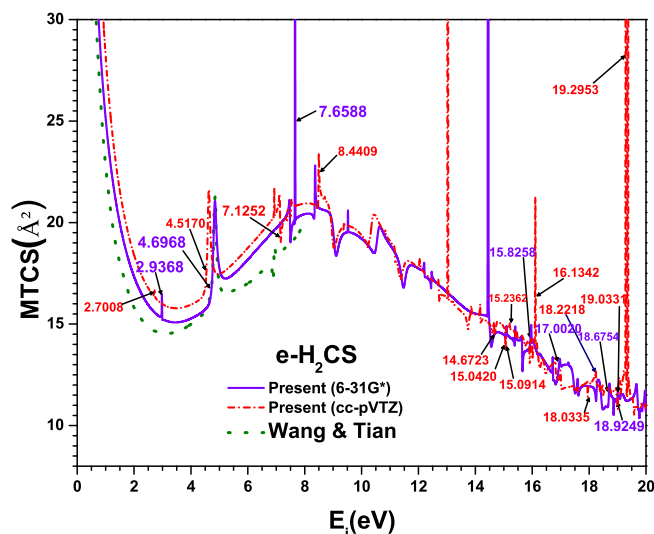


Fig. 8 (color online): Momentum Transfer Cross Section (MTCS) for $e - H_2CS$ scattering; Present: Solid - 6-31G* basis set, Short dash dot - cc-pVTZ basis set; Wang & Tian²⁰ - Dot

ditionally the peaks beyond 10 eV corresponds to other resonances as discussed in our eigenphase sum table.

Electron impact total ionization cross section is the most important fundamental quantity to many areas of applied interest. It is used as basic calibration data for a variety of analytical instruments such as ionization manometers, ionization chambers and mass spectrometers. Furthermore these quantities have the same basic significance for the initiation of reactions by ionizing radiation as do absorption coefficients for photo-chemical reaction initiation. In figure 9, we report our total ionization cross section for $e - H_2CS$ scattering using two methods, CSP-ic^{52,53} and BEB⁵⁵. There is excellent agreement between the data produced by two methods except at the peak. The BEB data have ionization cross section slightly higher compared to CSP-ic data at the peak. There are no other theoretical or experimental data to compare with our data. The maximum ionization cross section is 5 \AA^2 at 71 eV using CSP-ic method and 5.18 \AA^2 at 76 eV using BEB method. The numerical results of total ionization cross sections (from threshold to 5000 eV) for H_2CS are listed in Table 4.

In figure 10, we have compared total cross sections data for $e - H_2CS$ scattering using 6-31G* and cc-pVTZ basis sets with lone theoretical data of Wang and Tian²⁰. No other theoretical or experimental data are reported to the best of our knowledge. The total cross section calculation depends on the target model which in turn depends on the R-matrix radius in au (r), Number of states per symmetry (n) and Complete Active Space number (c). We performed series of calculations

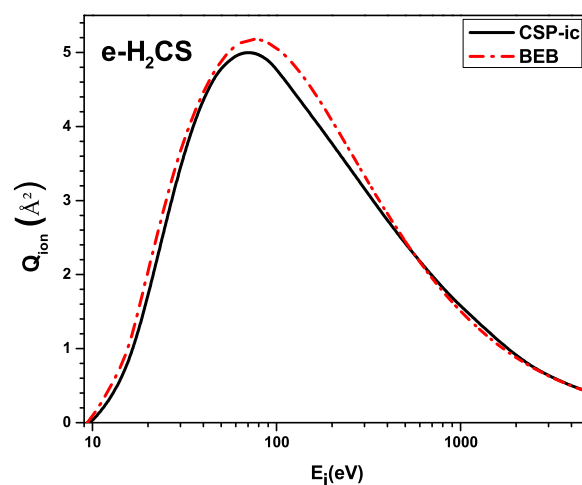


Fig. 9 (color online): Total Ionization Cross Sections for $e - H_2CS$ scattering; Solid line - CSP-ic method, Dash dot line - BEB method

Table 4 Total Ionization Cross Sections calculated using CSP-ic^{52,53} and BEB⁵⁵ Method

E_i eV	CSP-ic \AA^2	BEB \AA^2	E_i eV	CSP-ic \AA^2	BEB \AA^2
10	0.00	0.09	200	3.78	4.09
15	0.58	0.89	300	3.16	3.34
20	1.70	2.02	400	2.73	2.82
25	2.70	2.99	500	2.42	2.48
30	3.46	3.64	600	2.18	2.18
35	4.00	4.10	700	1.98	1.98
40	4.37	4.45	800	1.82	1.78
45	4.62	4.69	900	1.69	1.64
50	4.79	4.88	1000	1.58	1.52
60	4.97	5.10	2000	0.88	0.88
70	5.01	5.18	3000	0.63	0.63
80	4.98	5.16	4000	0.50	0.50
90	4.89	5.13	5000	0.41	0.41
100	4.78	5.07	-	-	-

and finalised two target model for computation of total cross section using two different basis sets viz. 6-31G* (Model 1 (M1) - c3n13r10) and cc-pVTZ (Model 2 (M2) - c3n16r10). We have taken the R-matrix radius to be 10 au in all the cases and observed the consistency of results. The numerical results of Total cross sections (from 0.01 eV to 5000 eV) using 6-31G* basis set are reported in Table 5.

It is now well evident that in case of polar molecules, due to the presence of long range dipole interaction, the total cross section at low energy is diverging in the fixed nuclei approximation. This is attributed to presence of singularity in the differential cross section in the forward direction. It is well known that the cross sections of dipole dominated processes only converge slowly with partial waves because of long range nature of the dipole potential. To obtain converged cross sections, the effect of rotation must be included along with a large number of partial waves. The higher partial waves ($l \geq 4$) are included using a Born correction as given in the work of Chu and Dalgarno⁵⁸. This is done by adjusting the T-matrices using the Close Coupling "CC" cross sections generated by the code POLYDCS³⁹. In this procedure our low l T-matrices are added to analytic dipole Born T-matrices using the adiabatic nuclear rotation (ANR)^{59,60}. The Born contribution for partial waves higher than $l = 4$ to the elastic cross section at energies below 1.5 eV is quite large as seen from Fig. 10.

Many structures and peaks observed in our eigenphase sum, momentum transfer curves are averaged out in total cross section curve below 10 eV. Our TCS results using 6-31G* basis set find excellent agreement with the SEP results of Wang and Tian²⁰. Our TCS results obtained using cc-pVTZ basis set are slightly higher compared to results of Wang and Tian²⁰ but qualitatively they follow the same shape as that of Wang and Tian²⁰. The core excited resonance peak is observed around 4.6 eV in TCS curve as a small peak using 6-31G* and cc-pVTZ basis set. Wang and Tian²⁰ also observed a small peak at 5.15 eV which is comparable with our peak in TCS curve around 4.6 eV. We observed a broad maximum around 10 eV in TCS curve using 6-31G* and cc-pVTZ basis sets and this may be attributed to fragmentation of the target. There is smooth transition in the TCS data obtained from R-matrix²⁴ using 6-31G* basis set and SCOP formalism^{41,44} at around 18 eV. Beyond 20 eV the data smoothly decreases and follows the Born Bethe term at higher energies. There are no data reported for TCS beyond 10 eV to compare our data with.

In Fig. 11 we present comparison of total cross section of Thioformaldehyde H_2CS , Formaldehyde H_2CO ²¹ and acetaldehyde CH_3CHO ²² because while there are no experimental data available, the theoretical comparisons are only till 10 eV. Due to the scarcity of TCS data on elastic scattering

with thioformaldehyde the following comparison may help us to understand the effect of functional groups on the structures observed at low energy. Resonance effect depends on the valence bonding order, electron negativity of atoms as well as the molecular geometry. Table 6 shows the comparison of various target properties of these targets. Comparison of functional group for these targets reveals that there is no carbonyl group in Thioformaldehyde against presence of carbonyl group in Acetaldehyde and Formaldehyde. We also know that Formaldehyde and Acetaldehyde contain the π^* unoccupied orbital on the C=O bond which are responsible for a shape resonance and this is not present in Thioformaldehyde and this may be the reason for absence of shape resonance at low energy below 3 eV. Replacing the CH_3 group in Acetaldehyde by a hydrogen atom is expected to lower the energy of the resonance since the CH_3 group donate electrons to the carbonyl chromophore more efficiently than an H atom. This is observed since the shape resonance peak for acetaldehyde is at 2.48 eV while that for formaldehyde is at 1.50 eV. The second significant observation is that all these molecular targets show second peak in their TCS curve at around 11 eV and they are mostly due to σ^* shape resonance. Further all these targets are polar in nature and that is reflected by a sharp rise (divergence) in the TCS curve at low energies. We also notice good agreement in TCS of thioformaldehyde and acetaldehyde²² beyond 10 eV. This may be due to the fact that they are isoelectronic (24 electrons) while TCS for formaldehyde is lower compared to these two molecular targets for all energy beyond 4 eV owing to smaller geometrical size of formaldehyde²¹. At higher energies beyond 1000 eV the TCS from all these targets tend to merge implying that at these energies cross sections do not depend much on structure but depends on the geometry and effective interaction time between the target and the electron. As energy increases the effective time of interaction decreases and hence the cross sections also decreases.

Finally electron impact scattering rate coefficients are plotted as a function of the kinetic temperature which is defined according to the Maxwell Boltzmann distribution. The collision rate coefficients can be interpreted as the cross-section times the thermal velocity. These rates have no selectivity and do not support any anomalous behaviour from their own. From this graph it is noted that the scattering rate increases rapidly up to approximately 300 K before gradually dying down as the temperature is further increased. The maximum rate coefficient value is $1.88 \times 10^{-6} \text{ cm}^3/\text{s}$. There is no data for comparison at reported temperature to the best of our knowledge.

Table 5 Total Cross Section (\AA^2) for the e - H_2CS Scattering

E_i (eV)	R- matrix	E_i (eV)	R- matrix	E_i (eV)	R- matrix	E_i (eV)	SCOP	E_i (eV)	SCOP
0.01	3291.28	1.60	30.29	8.00	29.10	19.0	24.26	600.0	5.68
0.05	596.57	1.80	28.60	8.50	29.90	20.0	23.33	700.0	5.23
0.10	289.93	2.00	27.25	9.00	30.35	30.0	21.79	800.0	4.86
0.20	145.43	2.50	25.00	9.50	30.58	40.0	19.69	900.0	4.54
0.30	99.75	3.00	23.65	10.00	30.50	50.0	17.92	1000	4.28
0.40	77.64	3.50	22.82	11.00	30.14	60.0	16.51	1500	3.33
0.50	64.67	4.00	22.45	12.00	29.71	70.0	15.52	2000	2.76
0.60	56.17	4.50	22.92	13.00	29.11	80.0	14.63	2500	2.37
0.70	50.16	5.00	24.05	14.00	28.45	90.0	13.89	3000	2.09
0.80	45.70	5.50	24.17	15.00	27.69	100	13.20	3500	1.87
0.90	42.25	6.00	24.77	16.00	26.84	200	9.56	4000	1.70
1.00	39.50	6.50	25.72	17.00	25.92	300	7.93	4500	1.56
1.20	35.40	7.00	26.96	18.00	25.16	400	6.93	5000	1.44
1.40	32.48	7.50	28.40	-	-	500	6.22	-	-

Table 6 Properties of targets

Target	Molecular Formula	IP eV	No. of electrons	Dipole moment ²³ (μ) in D	Bondlength (\AA) ²³ C=O Or C=S	C-R	Polarizability (α) ²³ \AA^3
Thioformaldehyde	H_2CS	9.38	24	1.647	1.611	1.087	5.721
Acetaldehyde	CH_3CHO	10.229	24	2.69	1.216	1.501	4.278
Formaldehyde	HCHO	10.885	16	2.33	1.205	1.111	2.77

4 Conclusion

We report detailed study of electron interaction on thioformaldehyde over an extensive range of impact energies. We employed ab initio R-matrix calculations for impact energies below 20 eV and above it spherical complex optical potential method is used. We employed fixed nuclei close coupling formalism with static exchange plus polarization model using 6-31G* and cc-pVTZ basis sets. The target properties obtained using 6-31G* and cc-pVTZ basis sets are in very good accord with earlier predicted results.

The present first electronic excitation energy of 1.88 eV is in good agreement with experimental value of 1.84 eV reported by Burton and Peyerimhoff¹⁵ and 1.80 eV measured by Judge et. al.¹⁰. The Eigenphase sum predicts resonance peaks and widths which are reported in Table 3, and find good agreement with earlier predicted data. The vertical excitation energies for excited states are in good agreement with the experimental results of Judge et. al.¹⁰, Judge and King⁹ and Drury et. al.¹¹ and theoretical results of MR-CI and Wang and Tian²⁰. Our DCS results (3 eV, 5 eV, 10eV and 20 eV), ionization cross section and scattering rate coefficient are reported for the first time. There is no theoretical TCS data beyond 10 eV and no experimental data for the total cross sections and hence reported for the first time. Due to sparse data for total cross sections we also reported comparison of total cross section of thioformaldehyde with formaldehyde and acetaldehyde

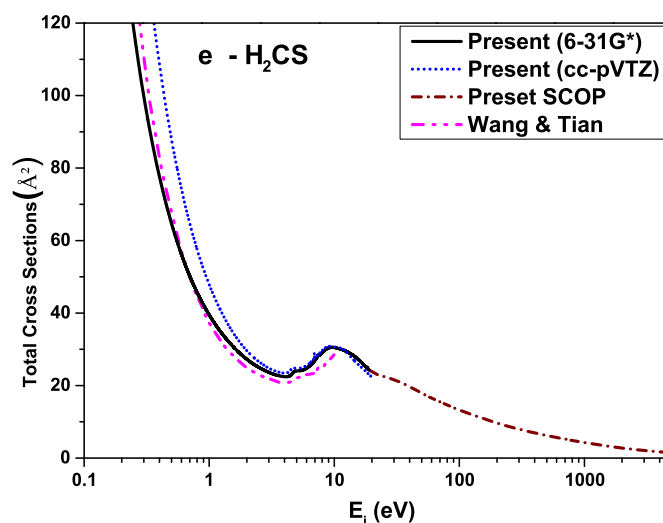


Fig. 10 (color online): e - H_2CS Total Scattering Cross Sections; Present R-matrix: Solid line - 6-31G* basis set, Short dot - cc-pVTZ basis set; Present SCOP formalism - Short dash dot; Wang & Tian²⁰: SEP cal. - Dash dot dot

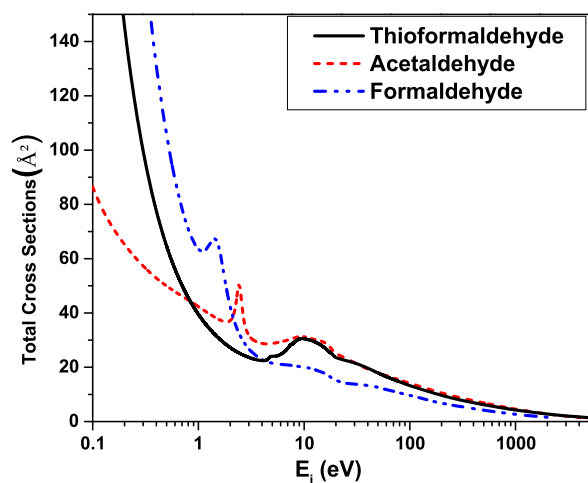


Fig. 11 (color online): Comparisons of Total Scattering Cross Sections for Thioformaldehyde (H_2CS) - Solid, Acetaldehyde (CH_3CHO)²² - Short dash and Formaldehyde ($HCHO$)²¹ - Dash dot dot

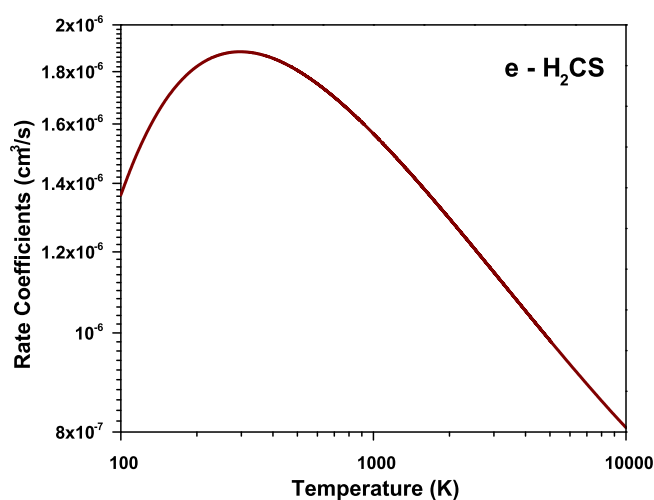


Fig. 12 (color online): total rate coefficients for $e - H_2CS$ elastic scattering

and carried out functional group study. The present work will inspire both theoreticians as well as experimentalist to investigate all the features for $e - H_2CS$ scattering reported in this paper.

5 Acknowledgement

Minaxi Vinodkumar and Chetan Limbachiya acknowledge DAE-BRNS, Mumbai for the Major research project [37(3)/14/44/BRNS-2014] for financial support under which part of this work is carried out.

References

- 1 M. Agundez, J. P. Fonfria, J. Cernicharo, J. R. Pardo, and M. Guelin, *Astron. Astrophys.* **479**, 493 (2008).
- 2 Y. C. Minh, W. M. Irvine, and M. K. Brewer, *Astron. Astrophys.* **244**, 181 (1991).
- 3 K. Willacy and T. J. Millar, *Astron. Astrophys.* **324**, 237 (1997).
- 4 S. D. Taylor, O. Morata, and D. A. Williams, *Astron. Astrophys.* **336**, 309 (1998).
- 5 J. I. Moses, M. Allen, and G. R. Gladstone, *Geophys. Res. Lett.* **22**, 1597 (1995).
- 6 B. E. Turner, *Astrophys. J.* **468**, 694 (1996).
- 7 K. Kasatani, M. Kawasaki, and H. Sato, *Chem. Lett.* **1**, 62 (2001).
- 8 Nummelin, P. Bergman, and A. Hjalmanson et al., *ApJS* **128**, p. 213 (2000).
- 9 R. H. Judge and G. W. King, *Can. J. Phys.* **53**, 1927 (1975).
- 10 R. H. Judge, D. C. Moule, and G. W. King, *J. Mol. Spectrosc.* **81**, 37 (1980).
- 11 C. R. Drury and D. C. Moule, *J. Mol. Spectrosc.* **92**, 469 (1982).
- 12 S. Y. Chiang and I. F. Lin, *J. Chem. Phys.* **122**, 094301 (2005).
- 13 H.C. Wu, C.C. Chen, and Y.T. Chen, *Spectrochim. Acta, Part A* **69**, 27 (2008).
- 14 P. J. Bruna, S. D. Peyerimhoff, R. J. Buenker, and P. Rosmus, *Chem. Phys.* **3**, 35 (1974).
- 15 P. G. Burton and S. D. Peyerimhoff, *Chem. Phys.* **73**, 83 (1982).
- 16 M. R. J. Hachey and F. Grein, *Can. J. Phys.* **73**, 18 (1995).
- 17 M. R. J. Hachey and F. Grein, *Chem. Phys.* **197**, 61 (1995).
- 18 M. R. J. Hachey and F. Grein, *J. Mol. Spectrosc.* **172**, 384 (1995).
- 19 F. Grein and M. R. J. Hachey, *Int. J. Quantum Chem.* **30**, 1661 (1996).
- 20 Y.F. wang and S.Xi Tian *Phys. Rev. A* **84**, 022790 (2011).
- 21 M. Vinodkumar, H. Bhutadia, B. Antony and N. Mason, *Phys. Rev. A*, **84**, 052701 (2011).
- 22 M. Vinodkumar, C. Limbachiya, H. Desai and P.C. Vinodkumar, *RSC Adv.* **5**, 69466 (2015).
- 23 <http://cccbdb.nist.gov>
- 24 D. Bouchiha, J. D. Gorfinkiel, L. G. Caron, and L. Sanche, *J. Phys. B: At. Mol. Opt. Phys.* **40**, 1259 (2007).
- 25 K. Kuchitsu (ed) "Structure of Free Polyatomic Molecules - Basic Data" Springer, Berlin, 1998
- 26 J. Tennyson, *J. Phys. B: At. Mol. Opt. Phys.* **29**, 6185 (1996).
- 27 J. Tennyson, *Physics Reports* **491**, 29 (2010).
- 28 J.D. Goddard, *Can. J. Chem.* **63**, 1910 (1985).
- 29 D. J. Clouthier, G. Huang, A. G. Adam, and A. J. Merer, *J. Chem. Phys.* **101**, 7300 (1994).
- 30 B. Fabricant, D. Krieger, and J. S. Muentzer, *J. Chem. Phys.* **67**, 1576 (1977).
- 31 D. R. Johnson, F. X. Powell and W. H. Kirchhoff, *Journal of Molecular Spectroscopy* **39**, 136 (1971).

- 32 R.H. Judge, C.R. Drury-Lessard and D.C. Moule, *Chem. Phys. Lett.* **53**, 82 (1978).
- 33 A.B. Callear, J. Connor and D.R. Dickson, *Nature* **221** (1969) 1238.
- 34 'Computational Methods for Electron Molecule Collisions', edited by W. M. Huo and F. A. Gianturco (Plenum, New York, 1995).
- 35 B. I. Schneider and T. N. Rescigno, *Phys. Rev. A* **37**, 3749 (1988).
- 36 T. N. Rescigno, C.W. McCurdy, A. E. Orel, and B. H. Lengsfeld III, in *Computational Methods for Electron Molecule Collisions*, edited by W. M. Huo and F. Gianturco (Plenum, New York, 1995), pp. 144
- 37 E. Jouscoski and M H F Bettega, *J. Phys. B: At. Mol. Opt. Phys.* **35**, 783 (2002).
- 38 J. Tennyson, C.J. Noble, *Comput. Phys. Comm.* **33**, 421(1984).
- 39 N. Sanna and F. A. Gianturco, *Comput. Phys. Commun.* **114**, 142 (1998).
- 40 F. A. Gianturco and A. Jain *Phys. Rep.* **143**, 347 (1986).
- 41 A. Jain, and K.L. Baluja, *Phys. Rev. A* **45**, 202 (1992).
- 42 M. Vinodkumar, H. Desai and P.C. Vinodkumar, *RSC Adv.*, **5**, 24564 (2015).
- 43 M. Vinodkumar, C. Limbachiya, H. Desai and P.C. Vinodkumar, *Phys. Rev. A* **89**, 062715 (2014).
- 44 M Vinodkumar, CG Limbachiya, KN Joshipura, NJ Mason, *The European Physical Journal D-Atomic, Molecular, Optical and Plasma Physics* **61**, 579 (2011).
- 45 H. L. Cox, and R. A. Bonham, *J. Chem. Phys.* **47**, 2599 (1967).
- 46 S. Hara, *J. Phys. Soc. Japan* **22**, 710 (1967).
- 47 X. Zhang, J. Sun, and Y. Liu, *J. Phys. B: At. Mol. Opt. Phys.* **25**, 1893 (1992).
- 48 *Handbook of Chemistry and Physics*, 76th ed., edited by D. R. Lide (CRC, Boca Raton, FL, 1995).
- 49 G. Staszewska, D. W. Schewenke, D. Thirumalai, and D. G. Truhlar, *Phys. Rev. A* **28**, 2740(1983).
- 50 M. Vinodkumar, K. Korot, P.C. Vinodkumar, *Int. J. of Mass Spectrometry* **305**, 26 (2011).
- 51 C. J. Joachain, *Quantum Collision Theory* (Amsterdam: North-Holland) (1983).
- 52 M Vinodkumar, C Limbachiya, H Bhutadia, *Journal of Physics B: Atomic, Molecular and Optical Physics* **43** (1), 015203 (2010).
- 53 M Vinodkumar, C Limbachiya, M Barot, M Swadia and A Barot, *Int. J. Mass Spect.* **339**, 16 (2013).
- 54 M. Vinodkumar, C. Limbachiya and H. Bhutadia *Journal of Physics B: Atomic, Molecular and Optical Physics* **43** (1), 015203 (2010).
- 55 Y. Kim and M. Rudd, *Phys. Rev. A* **50** 3954 (1994).
- 56 M. Vinodkumar, C. Limbachiya, H. Desai and P.C. Vinodkumar, *J. App. Phys.* **116**, 124702 (2014).
- 57 L. Andric, I. M. Cadez, R. I. Hall, and M. Zubeck, *J. Phys. B: At. Mol. Opt. Phys.* **16**, 1837 (1983).
- 58 S. I. Chu and A. Dalgarno, *Phys. Rev. A* **10**, 788 (1974).
- 59 N. T. Padiyal, D. W. Norcross, and L. A. Collins, *J. Phys. B: At., Mol. Opt. Phys.* **14**, 2901 (1981).
- 60 M. A. Morrison, *Adv. At. Mol. Phys.* **24**, 51 (1988).
- 61 P. D. Burrow and J. A. Michejda, *Chem. Phys. Lett.* **42**, 223 (1976).
- 62 S. Kaur and K. L. Baluja, *J. Phys. B* **38**, 3917 (2005).
- 63 T. N. Rescigno, C.W. McCurdy, and B. I. Schneider, *Phys. Rev. Lett.* **63**, 248 (1989).
- 64 T. C. Freitas, M. A. P. Lima, S. Canuto, and M. H. F. Bettega, *Phys. Rev. A* **80**, 062710 (2009).
- 65 C. Szmytkowski, *J. Phys. B*, **43**, 055201 (2010).